Inhalation Toxicology, 2009; 21(7): 607–618

informa
healthcare

RESEARCH ARTICLE

Dosimetry of nasal uptake of water-soluble and reactive gases: A first study of interhuman variability

Guilherme J. M. Garcia[1], Jeffry D. Schroeter[1], Rebecca A. Segal[2], John Stanek[3], Gary L. Foureman[3], and Julia S. Kimbell[1]

[1]The Hamner Institutes for Health Sciences, Research Triangle Park, North Carolina, [2]Virginia Commonwealth University, Richmond, Virginia, and [3]National Center for Environmental Assessment, U.S. Environmental Protection Agency, Research Triangle Park, North Carolina, USA

Abstract

Certain inhaled chemicals, such as reactive, water-soluble gases, are readily absorbed by the nasal mucosa upon inhalation and may cause damage to the nasal epithelium. Comparisons of the spatial distribution of nasal lesions in laboratory animals exposed to formaldehyde with gas uptake rates predicted by computational models reveal that lesions usually occur in regions of the susceptible epithelium where gas absorption is highest. Since the uptake patterns are influenced by air currents in the nose, interindividual variability in nasal anatomy and ventilation rates due to age, body size, and gender will affect the patterns of gas absorption in humans, potentially putting some age groups at higher risk when exposed to toxic gases. In this study, interhuman variability in the nasal dosimetry of reactive, water-soluble gases was investigated by means of computational fluid dynamics (CFD) models in 5 adults and 2 children, aged 7 and 8 years old. Airflow patterns were investigated for allometrically scaled inhalation rates corresponding to resting breathing. The spatial distribution of uptake at the airway walls was predicted to be nonuniform, with most of the gas being absorbed in the anterior portion of the nasal passages. Under the conditions of these simulations, interhuman variability in dose to the whole nose (mass per time per nasal surface area) due to differences in anatomy and ventilation was predicted to be 1.6-fold among the 7 individuals studied. Children and adults displayed very similar patterns of nasal gas uptake; no significant differences were noted between the two age groups.

Introduction

Human exposure to reactive gases and vapors is common since many such compounds have commercial use. Some of these compounds can be irritating or toxic to the respiratory system; examples include chlorine, formaldehyde, ozone, and hydrogen fluoride (Dahl, 1990; Morgan, 1994). Nasal absorption of inhaled gases that are water-soluble and reactive is expected to be high or moderate since the nasal passages are the main portal of entry to the respiratory system and have a large surface area lined with mucus. In fact, many reactive and water-soluble compounds are known to induce nasal tissue effects in laboratory animals (Dahl, 1990; Morgan, 1994; U.S. EPA, 1994), and the question is how to extrapolate these laboratory findings to human populations. To understand the health effects from such exposures on people, one needs to estimate the nasal dose in both animals and humans.

Nasal uptake of toxic gases depends on many factors, including nasal anatomy (differences among species; intraspecies interindividual variability such as gender or age differences), ventilation (inhalation rate; cyclic flow vs. unidirectional laboratory measurements), gas solubility, blood flow in the nasal mucosa, gas concentration in the environment, and properties of the chemical reactions of the gas in the nasal fluids and tissues (Morris, 1994). For inbred age-matched laboratory animal strains, variability in these factors is expected to be small. In humans, however, nasal anatomy shows considerable variation among individuals with respect to size, shape, and the presence or absence of anatomical abnormalities (Guilmette et al., 1997; Lang, 1989; Yokley, 2006). Ventilation rates are also affected by variations in age, body size, gender, and activity level (ICRP, 1994; Arcus-Arth & Blaisdell, 2007; Bide et al., 2000; Brochu et al., 2006). Finally, differences in

Address for Correspondence: Julia S. Kimbell, The Hamner Institutes for Health Sciences, 6 Davis Drive, PO Box 12137, Research Triangle Park, NC 27709, USA. E-mail: kimbell@thehamner.org

(Received 29 January 2008; revised 27 June 2008; accepted 03 July 2008)

ISSN 0895-8378 print/ISSN 1091-7691 online © 2009 Informa UK Ltd
DOI: 10.1080/08958370802320186

genetic background and general health status can lead to variations in the physical and chemical composition of the airway lining fluids and tissues, affecting metabolism and gas reactivity.

Computational fluid dynamics (CFD) studies using anatomically accurate nasal models have shown that the anatomical shape of the nasal passages affects the distribution of airflow inside the nose (Elad et al., 1993; Garcia et al., 2007; Morgan et al., 1991; Wexler et al., 2005). Since inhaled gases are transported in the nasal airspace by convection and diffusion, the amount of gas absorbed by different regions of the nose depends on airflow patterns and nasal anatomy. Let us consider the case of formaldehyde to illustrate how inhaled gases can be toxic to the respiratory tract. Formaldehyde has been shown to produce histopathological changes in the nasal mucosa of rats, monkeys, and mice exposed to concentrations of 6 ppm or higher (Naya & Nakanishi, 2005). Nasal cancer occurs in rats exposed to concentrations of 6 ppm or higher. In humans, chronic toxicity studies show loss of cilia, goblet-cell hyperplasia, and cuboidal and squamous cell metaplasia with regular exposure to 0.24 ppm in the workplace (Naya & Nakanishi, 2005).

Kimbell and colleagues developed CFD models of airflow and formaldehyde uptake in the noses of a rat, a monkey, and a human (Kimbell et al., 1993, 2001a, 2001b). The simulations predicted that formaldehyde flux (i.e., the rate at which formaldehyde is absorbed per unit surface area) from inspired air to nasal walls is distributed in a highly nonuniform manner throughout the nose, with a large anterior-to-posterior concentration gradient (Kimbell et al., 2001a). Comparisons of experimental data to simulated formaldehyde absorption rates showed that interspecies differences in the location of nasal lesions are associated with differences in the location of hotspots of formaldehyde absorption. Therefore, interindividual differences in nasal anatomy in the human population are expected to result in differences in airflow patterns, wall flux patterns, and total nasal uptake that may put certain age groups at higher risk of adverse effects when exposed to reactive, water-soluble gases.

While there have been no systematic studies of interhuman variability on gas uptake patterns in the nose, in vivo studies of nasal filtration of particles ranging from 0.5 to 10.0 μm in diameter revealed a great variability in the filtration efficiency among humans (Becquemin et al., 1991; Lehmann, 1935). For instance, Lehmann measured the nasal filtration efficiency of 0.5- to 2.0-μm particles in industry workers regularly exposed to silica-containing rock dust and in healthy volunteers (Lehmann, 1935). Nasal filtration in the healthy volunteers varied from 10% to 70% of the inhaled particles. Likewise, industry workers displayed a large variability in nasal filtration efficiency. Correlations with health status showed that industry workers with low nasal filtration were more susceptible to acquire silicosis than their counterparts with high nasal filtration. In another study, Becquemin and colleagues measured the deposition efficiency of 1.0-, 2.1-, and 2.8-μm particles in children, adolescents, and adults (Becquemin et al., 1991). They found that the noses of children did not filter the air as efficiently as those of adults. For instance, for 2.8-μm particles, 20 ± 11% of the inhaled particles were filtered in the adults, while only 11 ± 5% were extracted in the children during resting breathing. The present study raises the question of whether nasal uptake of inhaled gases is also different in children and adults, potentially putting one age group or another at higher risk for respiratory tract lesions when exposure occurs.

Federal guidelines for exposure to potentially toxic or irritating gases take into account both interspecies differences and interhuman variation. For example, in many of its risk assessments the U.S. Environmental Protection Agency (U.S. EPA, 1994) typically applies dosimetric adjustments to account for toxicokinetic differences between species as well as an uncertainty factor, typically 10-fold, to account for interhuman variation in both toxicokinetic and toxicodynamic processes (Dorne, 2004; Pelekis et al., 2003). The current "default" dosimetric procedure[1] used in estimating nasal dose of reactive, water-soluble gases to both animals and humans assumes complete and uniform uptake. This assumption is made in the absence of information on factors that may be of considerable influence, such as localized anatomical effects in the nasal passages, about which little quantitative information exists. Information on the variability of such factors is needed to assess whether this default method is adequately protective of human health.

This article describes the general nasal uptake patterns that are characteristic of reactive, water-soluble gases. It reports the extent of interhuman variability in nasal dose among five adults and two children. This is a first attempt to quantify, through CFD modeling, the variability of nasal dose due to differences in anatomy and ventilation in the human population and to examine whether certain age groups, in this case children, are at greater risk when exposed to toxic gases with either moderate or high nasal uptake. These results may be useful in developing and refining risk assessment guidelines for inhaled toxic gases to ensure confidence that they are adequately protective of health in human populations.

Methods

Construction of the CFD models

Five adults and two children were selected for this study. All subjects or their representatives signed a consent form agreeing with the use of their magnetic resonance imaging (MRI) or computed tomography (CT) scans. Nasal reconstructions of adults 1–4 were available from previous studies (Subramaniam et al., 1998; Segal et al., 2008), while the models of adult 5 and children 1–2 were developed for this project. A set of CT scans of the heads of 7 children was obtained from Materialise, Inc. (Ann Arbor, MI), while CT scans of adult 5 and an additional child were obtained

from medical collaborators. These scans were reviewed by an ear-nose-throat surgeon, who determined that, among the 8 children, only a 7-yr-old boy and an 8-yr-old girl had normal nasal anatomies. All adults were identified as normal nasal anatomies with no pathology. This dataset provided a range of body mass, gender, age (children vs. adults), and surface-area-to-volume ratio (Table 1), thus enabling the study of interhuman variability in gas uptake due to ventilation and anatomical differences. Inclusion of more subjects was not possible due to cost and time constraints.

The nasal geometries were captured by MRI scans of 3 mm spacing (adults 1–4) or CT scans of 0.4 to 0.7 mm spacing (adult 5 and children 1–2). The CFD models were created by two different methods. For adults 1–4, the nasal airway outlines on the scans were digitized and used to create three-dimensional hexahedral meshes of the nasal passages as described in detail elsewhere (Subramaniam et al., 1998; Segal et al., 2008). The resolution of the scan data was too coarse (3 mm between sections) to accurately resolve the nasopharynx in three of the individuals (adults 2, 3, and 4) and therefore an approximate nasopharynx was constructed for completeness (Figure 1). For this reason, most results reported in this article focus on the main nasal chamber (i.e., anterior to the nasopharyngeal region). The surface geometries of these hexahedral meshes were subsequently used to create tetrahedral meshes with higher element density in ICEM-CFD (Ansys, Inc., Canonsburg, PA) for use in this study.

The nasal geometries of adult 5, child 1, and child 2 were reconstructed in three dimensions from the CT scans using medical imaging software (Mimics, Materialise, Ann Arbor, MI) and were also meshed with tetrahedral elements in ICEM-CFD. The nasopharynx of child 2 was not scanned and therefore was also created manually for computational purposes (Figure 1). The quality of the tetrahedra was checked in ICEM-CFD to ensure that all cells had an aspect ratio larger than 0.3, a value needed to avoid distorted elements and optimize the accuracy of the numerical simulations. All meshes had from 2.4 to 3.5 million tetrahedral elements. A mesh density study was conducted to confirm that the results reported here are not dependent on mesh density. The nasal cavities were modeled as rigid structures.

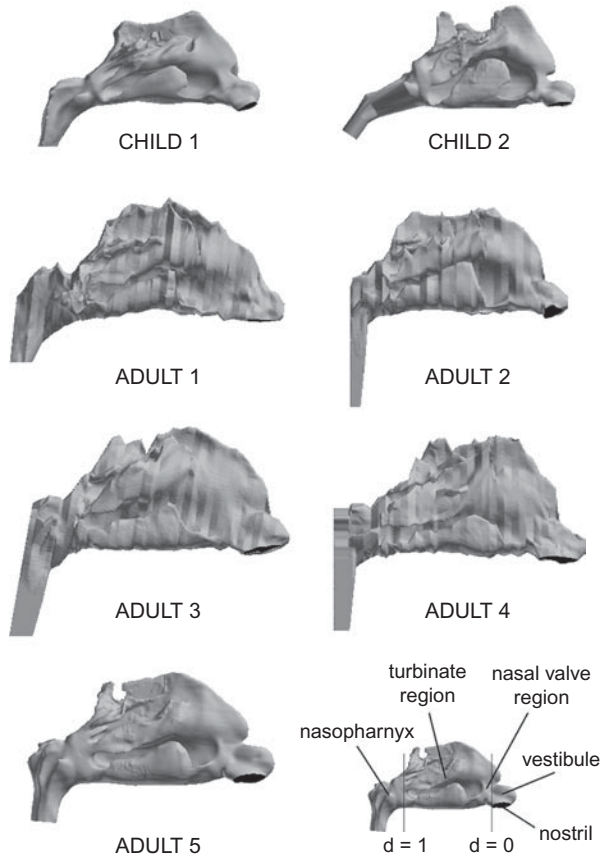

Figure 1. Geometry of the 7 nasal models (2 children and 5 adults) used in this study. The nostrils are to the right and the nasopharynx to the left. The nasopharynx is semi-artificial in Child 2 and Adults 2, 3 and 4. The normalized distance from the nostrils (d = Distance from nostrils/Length of the septum) is shown in the inset for d = 0 and d = 1.

Table 1. Anthropological data, geometric data, and the estimated minute volumes at rest for the two children and five adults included in the study.

	Children		Adults				
	Child 1	Child 2	Adult 1	Adult 2	Adult 3	Adult 4	Adult 5
Gender	Male	Female	Male	Female	Male	Female	Female
Age	7 years	8 years	53 years	—	—	—	37 years
Ethnicity	Asian	—	Caucasian	—	—	—	Caucasian
Body mass (kg) [a]	24.0	27.2	73	55.7	74	61.2	56.7
Allometrically scaled minute volume (L/min)—sitting awake [b]	5.5	5.8	9.0	6.8	9.0	7.1	6.9
SA of nasal cavity (mm^2) [c]	12,093	13,027	20,085	16,683	23,219	20,688	17,752
Volume of nasal cavity (ml) [c]	10.7	13.7	18.0	15.4	26.5	23.8	18.7
SAVR of nasal cavity (mm^{-1}) [c]	1.13	0.95	1.12	1.09	0.88	0.87	0.95
SA of nasal cavity + nasopharynx (mm^2)	14,469	15,590	24,327	21,968	27,994	24,243	20,448
Volume of nasal cavity + nasopharynx (ml)	18.3	20.8	33.3	26.8	46.5	35.9	29.1
Length from nostrils to end of septum (mm)	55.4	46.9	60.7	55.0	70.1	66.6	59.8

Note. SA, Surface Area; SAVR, surface-area-to-volume ratio.

[a]The body masses of the two children were estimated from age using data for U.S. children (ICRP, 1994); the data for the adults are measurements.

[b]Calculated with Eqs. (1) and (2). See Methods.

[c]The nasal cavity is defined as the region between the nostrils and the posterior end of the septum.

Statistical significance

The limited size of our sample (seven subjects) did not permit any statistical analysis of age- or gender-related differences in the nasal uptake of irritant gases and vapors. This study was designed to describe patterns of toxic gas absorption in several human noses and represents a preliminary assessment of the interindividual variability in these patterns. One should bear in mind that the creation of these computational models is labor-intensive and that this report is a significant increase in the number of subjects investigated in the nasal CFD literature, where most papers have examined airflow patterns and related transport processes in a single individual (Elad et al., 2006; Keyhani et al., 1995; Lindemann et al., 2005a, 2005b; Subramaniam et al., 1998; Zamankhan et al., 2006; Zhao et al., 2004).

Airflow simulations

A major determinant of respiratory-tract dose in humans exposed to inhaled gases is ventilation since it determines the residence time of the gas. Unfortunately, precise values of the breathing rates of children in narrow age ranges performing different activities are still unknown (Arcus-Arth & Blaisdell, 2007). Such measurements are difficult because breathing pattern is affected by the use of a mouthpiece (Perez & Tobin, 1985) and by the subject being aware of the recording (Han et al., 1997). Furthermore, bulky equipment makes direct measurements impractical in children performing typical activities during an entire day (Arcus-Arth & Blaisdell, 2007).

To overcome these difficulties, the most comprehensive reports to date used indirect data, such as food intake or disappearance rates of deuterium (^{2}H) and heavy oxygen-18 (^{18}O), to estimate daily O_2 consumption or CO_2 production, thus allowing the computation of daily averages of breathing rates in humans of all ages (Arcus-Arth & Blaisdell, 2007; Brochu et al., 2006; Layton, 1993). Although these reports provide ventilation rates for narrow age groups, only daily breathing rates are provided instead of ventilation at rest. In acknowledgment of the changes in breathing rates with activity level, we opted to use the ICRP report (ICRP, 1994) as our source for breathing rates, the estimates for which are close to the radioisotope depuration method (Brochu et al., 2006) (Figure 2A).

The ICRP report provides breathing rates for adults and children aged 0.25, 1, 5, 10, and 15 yr under different activity levels (sleeping, sitting awake, light exercise, and heavy exercise) (ICRP, 1994). We simulated airflow and uptake patterns for people sitting awake. Our results are also descriptive of other sedentary activities for which the level of ventilation is low, such as watching TV or driving a car (Beals et al., 1996). In agreement with other studies (Aitken et al., 1986; Beals et al., 1996; Layton, 1993), the ICRP report provides minute volumes (amount of air exhaled in 1 min) that are smaller in adult females than in adult males of the same body size, while no gender difference is acknowledged in children 10 yr old and younger. Therefore, assuming that the relationship between minute volume and body mass is a power law,

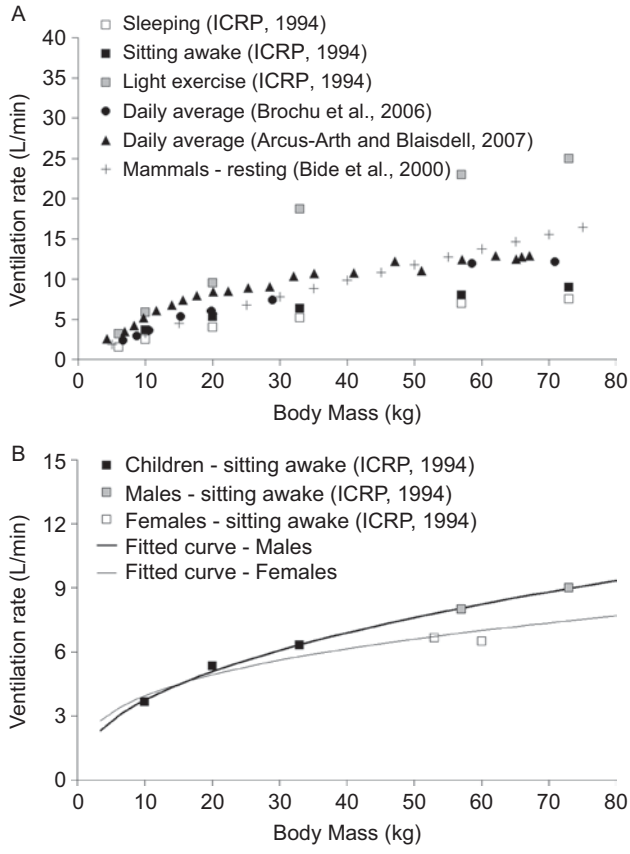

Figure 2. (A) Comparison of the ventilation rates in humans at three different activity levels (sleeping, sitting awake and light exercise) from the ICRP report with more recent reports of the breathing rates in humans and mammals. (Only the male data is shown for simplicity.) Daily averages are higher than rates for people sitting awake, as expected. The allometric equation for resting mammals overpredicts resting airflow in humans greater than 30 kg. (B) Curve fits to the ICRP data for males and females sitting awake (equations (1) and (2)).

we fitted separate equations to describe the male and the female data (Figure 2B):

Males (sitting awake):

$$\dot{V}_E = (1.36 \pm 0.10) M^{0.44 \pm 0.02} \quad r = 0.995 \tag{1}$$

Females (sitting awake):

$$\dot{V}_E = (1.89 \pm 0.40) M^{0.32 \pm 0.06} \quad r = 0.897 \tag{2}$$

where $\dot{V}_E$ is the minute volume in liters per minute, M is the body mass in kilograms, and r is the correlation coefficient.

The body masses of the adults were known, while for the two children they were estimated from age using data from the ICRP report (Table 1). The minute volumes for the children were calculated using Eq. (1) because it provided a better fit to the children's data (Figure 2B) and because no gender differences among children are noted in the ICRP report. The results, 5.5 L/min for the 7-yr-old boy and 5.8 L/min for the 8-yr-old girl, are similar to the average minute volume of 6.1 ± 1.7 L/min obtained by Bennett and Zeman (2004) using respiratory inductance plethysimography on a study of 36 children aged 6 to 13 yr (mean of 10 ± 2 yr). The minute volumes of the adults, ranging from 6.8 to

9.0 L/min, are also in good agreement with literature values (Han et al., 1997; Layton, 1993; Perez & Tobin, 1985).

Simulations of steady-state inspiratory airflow were conducted using the commercially-available CFD software package Fluent (Fluent, Inc., Lebanon, NH). Details on the differential equations solved, computational algorithms employed, and boundary conditions and physical properties utilized can be found in the Appendix. Mean inspiratory airflow rates were calculated by assuming that the duration of inspiration and expiration are the same, so that the inspiratory airflow rates used in the simulations were twice the minute volumes obtained with equations (1) and (2). Since reactive, water-soluble gases evading nasal filtration are readily extracted by the pharynx, larynx, trachea, and lung airways, nasal gas absorption during expiration was assumed to be small and therefore was not simulated. Airflow simulations using some of the CFD models employed here (adults 1–4) have been previously compared with dye-streakline analyses in hollow molds constructed from the CFD geometries and showed good agreement with experimental measurements (Segal et al., 2008).

Gas uptake simulations

A broad spectrum of physicochemical properties is observed in gases that are toxic to humans (Dahl, 1990; U.S. EPA, 1994). Highly reactive and water-soluble gases are quickly converted to nonvolatile products in mucus, so their effects are largely confined to the nasal tissues. On the other end of the spectrum, gases with low reactivity reach the circulatory system and, if metabolized by enzymes, may produce metabolites that are toxic to tissues distant from the respiratory tract. The results presented here are representative of reactive, water-soluble gases with moderate to high nasal uptake. Formaldehyde, chlorine, and hydrogen fluoride are examples of gases with high nasal uptake, while ozone, sulfur dioxide, and xylene are examples of gases with moderate nasal uptake (U.S. EPA, 1994). Gases with moderate nasal uptake are not entirely scrubbed by the nasal mucosa and reach the lower respiratory tract in greater doses than gases with high nasal uptake.

One should bear in mind that each specific gas undergoes specific chemical reactions with the nasal epithelium, with a given chemical frequently reacting preferentially with a specific epithelium type (squamous, transitional, respiratory, or olfactory). To produce chemical-specific models of gas uptake in the nose, it is necessary to know (a) the three-dimensional location of each epithelial type and (b) how a particular gas reacts with each epithelial type (Carey et al., 2007). Since none of these items can be fully addressed with the data currently available, we chose to model a generic gas by assuming a uniform boundary condition throughout the nose. Therefore, the reader should keep in mind that the uptake patterns for a given gas may be quite different from those reported here if that gas reacts preferentially with one specific epithelial type.

Simulations of nasal uptake of inhaled gas were conducted in Fluent. Gas concentration in ambient air was defined to be 1.0 ppm by volume (1.227×10^{-6} kg/m^3) and set as a boundary condition at the nostrils. The gas diffusivity was defined to be $D = 1.5 \times 10^{-5}$ m^2/s, which is the estimated air-phase diffusivity of formaldehyde (Hobler, 1966; Kimbell et al., 2001a). The diffusivity of other reactive gases, such as ozone or chlorine, usually lies in the range 1×10^{-5} to 5×10^{-5} m^2/s.

The boundary conditions used to simulate moderate and high (maximum) nasal uptake were:

Boundary condition no. 1: Maximum uptake. Assuming an infinitely fast reaction of absorbed gas with compounds in the airway lining, gas concentration was set to zero at the airway walls ($c = 0$ at the walls).

Boundary condition no. 2: Moderate uptake. To simulate a chemical reaction with a finite rate constant at the nasal walls, the rate of gas absorption at the walls (i.e., wall mass flux) was defined to be proportional to the gas concentration in air adjacent to the wall, which in mathematical terms means (Taylor, 2006):

$$\text{Flux} = -D(\vec{n} \times \nabla c)_{\text{wall}} = k(c)_{\text{wall}} \tag{3}$$

Here Flux is the wall mass flux of inhaled gas, c is the gas concentration in air, ∇c denotes the gradient of c, $\vec{n}$ is a unit vector perpendicular to the wall, and k is a constant. The constant k is a measure of how soluble and reactive in the nasal lining the gas is (Cohen Hubal et al., 1996; Taylor, 2006). In the context of the U.S. EPA reference concentration (RfC) methodology (U.S. EPA, 1994), k is proportional to the product of the mass transport coefficient in the mucus/tissue phase (k_l) and the mucus/tissue:air partition coefficient ($H_{t/g}$). The proportionality constant between k and $k_l H_{t/g}$ depends on gas diffusivity in the mucus/tissue phase, mucus/tissue thickness, and the first-order reaction constant.

An alternative approach to obtain k is to develop computational models of the nasal passages of laboratory animals and calculate k by fitting the total nasal uptake predicted by the model to experimental measurements. This approach was used by Kimbell and colleagues (Kimbell et al., 2001a, 2001b) to describe nasal uptake of inhaled formaldehyde in rats, monkeys, and humans. To simulate moderate uptake in the current study, the constant k was adjusted so that 80% of the inhaled gas was absorbed in the nose of adult 1. The value obtained, namely, k = 4.93 cm/s, was applied to all other subjects.

Analysis of results

To describe the patterns of nasal uptake of inhaled gases, cross-sectional averages of gas concentration in air and perimeter averages of gas absorption rates (wall fluxes) were plotted as a function of the distance from the nostrils. In order to facilitate comparison among individuals, the distance from the nostrils was normalized by the septal length, which was defined as the linear distance from the first coronal cross-section after the nostrils to the coronal section where the septum ends (Figure 1). The data for the five adults and two children were averaged into two separate groups to aid visualization. The surface area of the models

was divided into three regions, namely, the left cavity, the right cavity, and the nasopharynx, by means of a coronal section at the end of the septum. This allowed averages and maximum values of the wall fluxes to be computed separately for each of these regions.

In order to describe the percentage of nasal surface area with wall mass fluxes in a given range, the distribution of surface area by flux values was investigated for both maximum and moderate extraction scenarios. For each uptake scenario, the range from 0 to the maximum wall mass flux was evenly divided into N partitions, or bins. (Here we used $N = 20$.) The percentage of nasal surface area with flux values corresponding to each bin was calculated (Kimbell et al., 2001b). The average value of the wall mass flux in each bin is given by

$$\text{Flux} = \left(\frac{\text{Bin number} - 0.5}{\text{N}}\right)\text{Flux}_{\text{max}} \tag{4}$$

where Bin number = 1, 2, . . . , N and Flux_{max} is the maximum flux for each individual. This process allowed the distribution of surface area by flux magnitude to be compared among individuals and uptake scenarios.

Finally, we note that, although the simulations presented here considered an ambient concentration of 1 ppm, wall fluxes for other ambient concentrations can be calculated by multiplying the results presented here by the desired ambient concentration in ppm. For instance, a wall flux calculated to be 2×10^{-8} kg/s-m^2 in the 1-ppm simulations would become 4×10^{-8} kg/s-m^2 for an ambient concentration of 2 ppm. This procedure is valid because both the boundary condition applied and the convection-diffusion equation governing gas transport (see Appendix) are linear. The reader should note, however, that a linear relationship between wall flux and inspired concentration should not be expected after the specific chemical reactions of a given gas with the nasal lining are taken into account. Factors such as the availability of mucus substrates or enzymatic chemical reactions lead to nonlinearities, as has been observed for nasal uptake of hydrogen sulfide (Schroeter et al., 2006a, 2006b).

Results

Anatomical variability among the five adults and two children is described in Table 1. The surface area, volume, and length of the nasal cavity from the nostrils to end of the septum were smaller in the children than in the adults (121–130 cm^2 vs. 167–232 cm^2, 10.7–13.7 ml vs. 15.4–26.5 ml, 4.7–5.5 cm vs. 5.5–7.0 cm, respectively). Although the nasal cavities of the children were smaller in surface area, volume and length, the surface-area-to-volume ratios (SAVR) were similar in the two age groups (0.95–1.13 mm^{-1} vs. 0.87–1.12 mm^{-1}). To assess whether our small sample of seven subjects provided a reasonable range of anatomical variability, we compared our numbers with literature data. Guilmette and coworkers (1997) used MRI scans of 45 adults to estimate the nasal surface area. Their average surface area of 183 ± 22 cm^2 is in good agreement with the range of values for the adults in our sample. Yokley (2006) used CT scans of 40 adult Caucasians to investigate nasal anatomy. His result SAVR = 1.05 ± 0.23 mm^{-1} is in good agreement with the range in our sample. These comparisons showed that our group of five adults has a reasonable amount of anatomical variability, although it does not include the full range of variability observed in studies with larger data sets. A detailed comparison of specific anatomical landmarks among the children and adults was beyond the scope of this project, but coronal cross sections of the nasal anatomy suggested that the general shape of the nasal cavity was the same in both groups (Figure 3).

The simulations predicted that, under both boundary conditions, gas was rapidly absorbed by the nasal mucosa once it entered the nostrils (Figures 3 and 4). At the location where the septum ends and the right and left cavities merge, gas concentration in inspired air had dropped to ~13% and ~29% of the inlet concentration for the maximum and moderate uptake scenarios, respectively. The simulations also predicted some interhuman variability in the gas concentration at all levels. For instance, halfway between the nostrils and the end of the septum, gas concentration in air varied from 0.24 ppm to 0.42 ppm for the maximum uptake conditions and from 0.43 ppm to 0.61 ppm for the moderate uptake conditions among the 7 subjects investigated.

Total nasal extraction under maximum uptake conditions was predicted to vary from 89.2% to 93.5% in the 5 adults studied, with an average of 91.9%, while in the 2 children the values were 88.2% and 92.0% with an average of 90.1% (Table 2). These results suggest that even if one assumes that gas absorption by the nasal mucus and

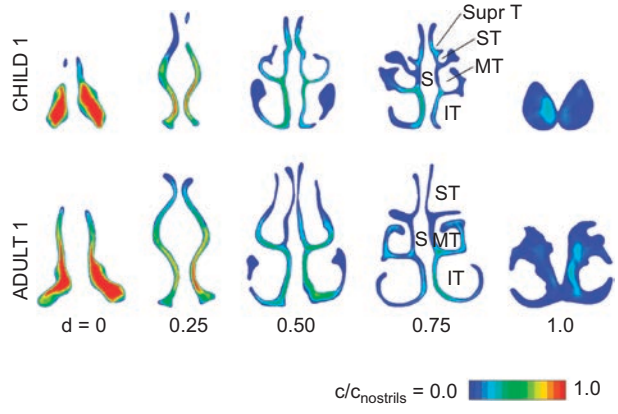

Figure 3. Coronal cross-sections of the nasal cavity of a 7-year-old child and an adult colored by gas concentration. The normalized distance from the nostrils (d = Distance from nostrils/Length of the septum) is given for each cross-section. The gas concentration c is given as a fraction of the concentration at the nostrils ($c_{nostrils}$) assuming $c = 0$ at the walls (Boundary Condition no. 1 - Maximum uptake). The anatomical landmarks are: S = septum, IT = inferior turbinate, MT = middle turbinate, ST = superior turbinate, Supr T = supreme turbinate.

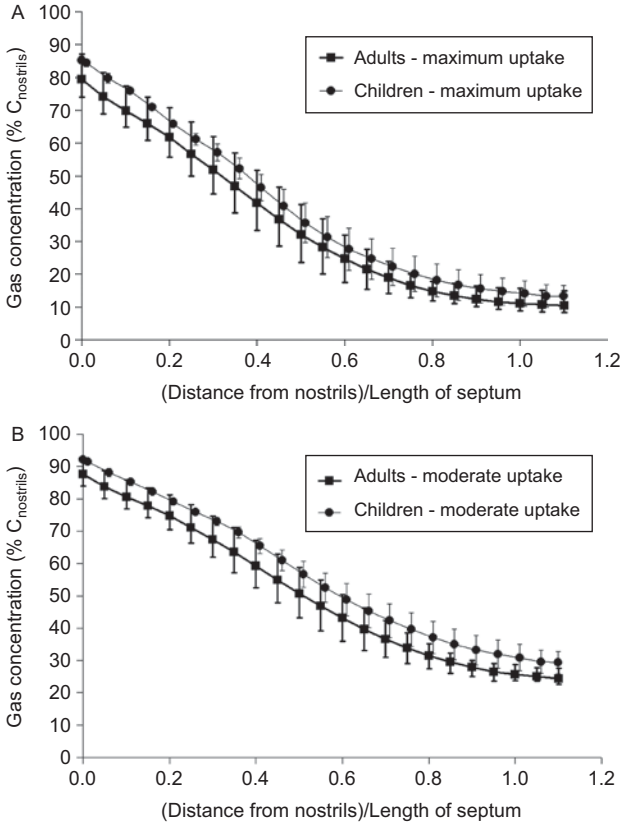

Figure 4. Average gas concentration as a distance from the nostrils. The first coronal cross-section after the nostrils (see Figs. 1 and 3) was defined as the origin and the distance was normalized by the septal length of each subject (Table 1). The averages for the 5 adults and 2 children included in this study are shown; the vertical bars show the range of variation in each group. (A) Boundary Condition no. 1: maximum uptake. (B) Boundary Condition no. 2: moderate uptake.

Table 2. Total gas uptake during resting breathing in the seven humans investigated under conditions of maximum uptake (Boundary Condition no. 1) and moderate uptake (Boundary Condition no. 2).

	Total gas uptake	
Subject	Maximum uptake	Moderate uptake
Adult 1	93.5%	80.0%
Adult 2	92.4%	80.5%
Adult 3	93.1%	81.4%
Adult 4	89.2%	77.4%
Adult 5	91.5%	78.2%
Child 1	92.0%	77.2%
Child 2	88.2%	73.3%

reaction with its constituents are infinitely fast, approximately 10% of the inhaled gas can still traverse the nasal cavity, reaching the larynx and possibly the proximal lung airways (Overton et al., 2001). Under moderate extraction conditions, an even larger proportion of inhaled gas was predicted to traverse the nose, with total nasal uptake varying from 77.4% to 81.4% in the adults and 73.3% to 77.2% in the children (averages were 79.5% and 75.3%, respectively).

The spatial patterns of gas uptake in the nasal cavity were predicted to be highly nonuniform with most of the gas being

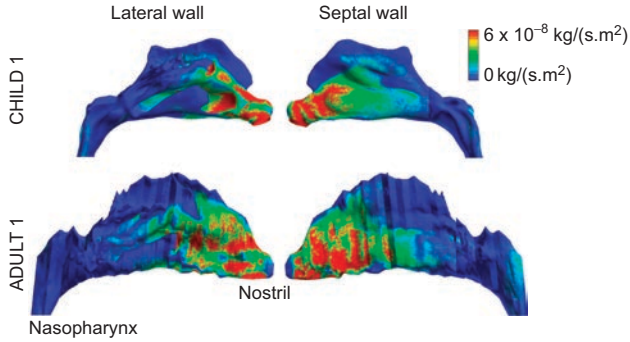

Figure 5. Spatial distribution of gas absorption rates along the nasal wall in one child and one adult under maximum uptake boundary conditions (Boundary Condition no. 1). Only the right cavity and the nasopharynx are displayed. The models are shown with the correct relative scaling. To aid visualization, the maximum value of the color-map scale was set to 6×10^{-8} kg/(s.m^2), although wall fluxes were greater than that in some small areas (see the maximum flux values on Tables 3). Areas where flux exceeds 6×10^{-8} kg/(s.m^2) are displayed in red.

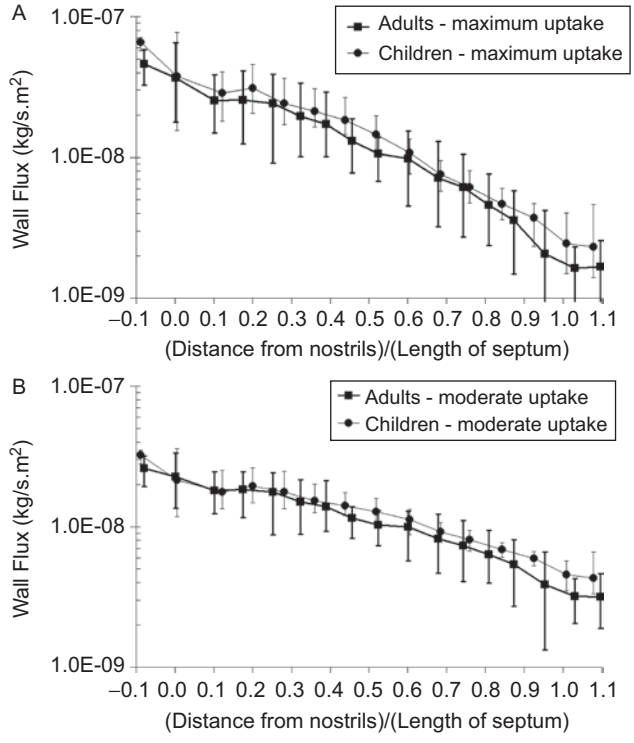

Figure 6. Wall fluxes (or rates of gas absorption) as a distance from the nostrils. The first coronal cross-section after the nostrils (see Figs. 1 and 3) was defined as the origin and the distance was normalized by the septal length of each subject (Table 1). The averages for the 5 adults and 2 children included in this study are shown; the vertical bars show the range of variation in each group. (A) Boundary Condition no. 1: maximum uptake. (B) Boundary Condition no. 2: moderate uptake.

absorbed in the anterior portion of the nose (Figures 5 and 6). Although minute volumes are smaller in children than in adults (Table 1), meaning that children inhale less gas for a given period of exposure than adults, the simulations predicted rates of gas absorption per unit of surface area of comparable magnitude in the two age groups (Figure 6).

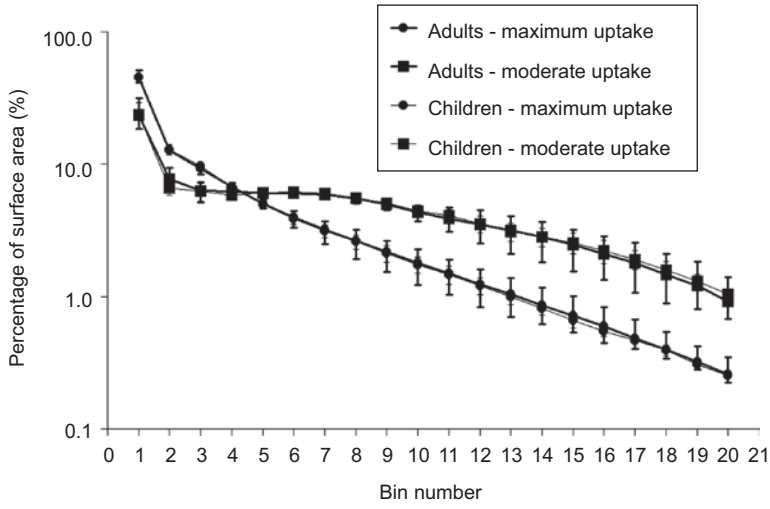

Figure 7. Percentage of surface area of the nose (left and right cavities only; nasopharynx excluded) by magnitude of gas absorption rate. The surface area of the nose was split into 20 bins. The wall flux is minimum for Bin number = 1 and maximum for Bin number = 20. The flux values corresponding to each bin can be calculated by substituting in Equation 4 the maximum fluxes ($Flux_{max}$) for each individual (Tables 3 and 4). See caption of Fig. 4 for description of symbols.

Table 3. Simulation results for the average and maximum wall fluxes (gas absorption rates) for maximum uptake (Boundary Condition no. 1) conditions.

	Average flux (10^{-8} kg/sm^2)		Maximum flux (10^{-8} kg/sm^2)	
Subject	Left cavity	Right cavity	Left cavity	Right cavity
Adult 1	1.8	1.5	10.8	10.0
Adult 2	1.5	1.5	10.8	10.4
Adult 3	1.6	1.3	11.0	10.6
Adult 4	1.2	1.2	10.6	10.2
Adult 5	1.4	1.5	10.8	10.0
Child 1	1.9	1.5	11.8	11.0
Child 2	1.6	1.5	12.3	11.6

Table 4. Simulation results for the average and maximum wall fluxes (gas absorption rates) for moderate uptake (Boundary Condition no. 2) conditions.

	Average flux (10^{-8} kg/sm^2)		Maximum flux (10^{-8} kg/sm^2)	
Subject	Left cavity	Right cavity	Left cavity	Right cavity
Adult 1	1.4	1.3	4.4	4.4
Adult 2	1.2	1.2	4.4	4.4
Adult 3	1.3	1.1	4.6	4.6
Adult 4	1.0	1.0	4.6	4.4
Adult 5	1.2	1.2	4.6	4.4
Child 1	1.5	1.2	4.6	4.6
Child 2	1.2	1.2	4.8	4.6

Significant interhuman variability in flux values at specific points on the walls was predicted due to the differences in anatomy and ventilation (Figure 6), although total uptake (Table 2) and whole-nose fluxes (Tables 3 and 4) were quite similar among subjects.

Of particular interest are the regions where the rate of gas absorption was predicted to peak, since these regions likely correspond to areas of increased risk of tissue damage. The maximum rates of gas absorption were located in the front of the nose or in the anterior end of the inferior and middle turbinates and were generally of similar magnitude in the left and right nasal cavities (Figure 5; Tables 3 and 4). In the maximum uptake scenario, maximum values of wall flux were 6–9 times greater than the average flux over the entire surface area. In the moderate uptake scenario, maximum values of wall flux were 3–5 times greater than average. Maximum wall fluxes were greater in the maximum uptake scenario than in the moderate uptake scenario (Tables 3 and 4).

The distribution of nasal surface area by wall flux magnitude was different for the maximum and moderate uptake scenarios (Figure 7; Table 5). Although in both scenarios the spatial distribution of wall fluxes was highly nonuniform, the distribution was more nonuniform under maximum uptake than under moderate uptake. For instance, in the maximum uptake scenario, 45% of the total surface area of the nose was predicted to receive fluxes under 5% of the maximum flux (Bin number 1), while only 1.5% of the surface area was computed to be exposed to fluxes greater than 80% of the maximum flux (Bin numbers 17–20). In contrast, under moderate uptake conditions, only 24% of the surface area received fluxes below 5% of the maximum value, while 5.5% of the surface area had fluxes greater than 80% of the maximum flux (Figure 7; Table 5).

Discussion

Wall flux is a surface area-based dose metric with units of mass/(time-area) and, when available, may be used in the current U.S. EPA RfC methods to estimate nasal dose in general (U.S. EPA, 1994). The U.S. EPA RfC methods estimate nasal dose as the mean wall flux throughout the entire nasal mucosa, namely (exposure concentration) × $\dot{V}_E$/SA, where $\dot{V}_E$ is the minute volume and SA is the nasal surface area. This formula assumes complete nasal extraction with a uniform flux throughout the nasal passages.

Table 5. Distribution of the surface area of the nose (left and right cavities only; nasopharynx excluded) into 20 bins by magnitude of wall fluxes.

(A) Maximum uptake (Boundary Condition no. 1)

	Adults			Children		
	Percentage of surface area (%)			Percentage of surface area (%)		
Bin number	Average	Maximum	Minimum	Average	Maximum	Minimum
1	45.08	51.11	41.19	45.11	46.81	43.40
2	12.72	13.00	12.25	12.93	14.16	11.70
3	9.25	9.95	8.40	9.69	9.94	9.44
4	6.73	7.20	6.45	6.65	6.99	6.32
5	5.04	5.37	4.66	5.00	5.39	4.61
6	3.94	4.44	3.31	3.88	4.24	3.52
7	3.21	3.72	2.48	3.14	3.48	2.79
8	2.65	3.18	1.93	2.61	2.94	2.28
9	2.18	2.65	1.53	2.13	2.45	1.82
10	1.80	2.27	1.22	1.74	2.00	1.49
11	1.50	1.91	1.03	1.47	1.71	1.24
12	1.23	1.59	0.84	1.21	1.38	1.03
13	1.04	1.39	0.70	0.99	1.12	0.87
14	0.86	1.17	0.62	0.82	0.91	0.72
15	0.71	1.01	0.54	0.66	0.75	0.58
16	0.60	0.83	0.45	0.55	0.60	0.50
17	0.48	0.67	0.40	0.47	0.50	0.44
18	0.40	0.54	0.34	0.39	0.43	0.35
19	0.32	0.42	0.28	0.31	0.33	0.29
20	0.26	0.35	0.22	0.25	0.26	0.25

(B) Moderate uptake (Boundary Condition no. 2)

	Adults			Children		
	Percentage of surface area (%)			Percentage of surface area (%)		
Bin number	Average	Maximum	Minimum	Average	Maximum	Minimum
1	23.56	31.59	18.52	23.77	29.01	18.53
2	7.72	9.37	6.14	6.63	7.47	5.80
3	6.33	7.31	5.17	6.23	7.17	5.28
4	6.25	6.98	5.45	5.82	5.92	5.71
5	6.03	6.51	5.71	6.07	6.54	5.60
6	6.01	6.43	5.71	6.19	6.69	5.68
7	5.89	6.41	5.44	6.02	6.37	5.67
8	5.52	5.99	5.01	5.54	5.75	5.34
9	5.00	5.28	4.48	5.10	5.54	4.66
10	4.36	4.83	3.70	4.45	4.93	3.97
11	3.90	4.72	3.09	4.10	4.54	3.65
12	3.48	4.47	2.52	3.54	4.04	3.04
13	3.16	4.07	2.11	3.10	3.59	2.61
14	2.82	3.66	1.81	2.83	3.26	2.39
15	2.47	3.21	1.55	2.56	3.01	2.10
16	2.11	2.84	1.33	2.22	2.66	1.78
17	1.80	2.54	1.07	1.91	2.21	1.60
18	1.47	2.10	0.89	1.59	1.84	1.35
19	1.20	1.83	0.80	1.31	1.46	1.15
20	0.92	1.40	0.67	1.04	1.14	0.94

Note. Wall fluxes are minimum for Bin number = 1 and maximum for Bin number = 20; the flux values corresponding to each bin can be calculated with Eq. (4). Averages for adults and children are reported as well as maximum and minimum values for each group. The data are plotted in Figure 7.

Since nasal extraction under maximum uptake conditions was close to 90% (Table 2), the average wall fluxes predicted for boundary condition no. 1 (Table 3) are very similar to those that would have been predicted assuming complete extraction with a uniform flux throughout the entire nasal passages. The simulations, however, showed that such an approach would be a significant simplification of the problem. Absorption rates are much higher in the anterior nose than in posterior regions (Figure 6), so that the wall fluxes can be up to nine times greater than average in hotspots of gas absorption (Table 3). These effects are important in developing dose-response models for inhalation toxicology that are capable of describing local phenomena, such as the location of nasal lesions (Kimbell et al., 2001a, 2001b).

A second limitation of the U.S. EPA RfC methods (1994) is that wall flux is not always the best dose metric (Dahl, 1990). Wall flux may be an appropriate dose metric for a direct-acting cytotoxicant like formaldehyde, but other metrics, such as tissue concentration (with units of mass/volume of tissue), may be more appropriate to other modes of action for toxic response, such as non-parent-compound toxicity and toxicity that is metabolically mediated (Dahl, 1990; Andersen & Jarabek, 2001). The U.S. EPA RfC methods do not currently quantitatively account for the different modes of action for toxic responses (U.S. EPA, 1994).

Interindividual variation in the average and maximum wall fluxes over the entire nasal mucosa was less than 1.6-fold in our simulations (child 1 vs. adult 4; Table 3). Although this result applies only to this small population of seven individuals, it provides a preliminary indication that differences in anatomy and minute volume may contribute less than twofold to interindividual variation in whole-nose dose. One must note, however, that there are other sources of interindividual variability on the toxic effects of inhaled gases. We investigated only toxicokinetic effects (differences in distribution and magnitude of absorption rates along the wall). However, interindividual differences in toxicodynamics (how the chemical reacts with biological compounds) are also expected, for instance, due to genetic differences in metabolite concentration. These differences in toxicodynamics may also influence gas uptake rates by modifying the gas concentration gradient from the air phase to the mucus/tissue phase.

The greater variability among individuals seen for wall fluxes at specific sites of the nasal passages (Figure 6) in comparison to the minimal variability in total uptake (Table 2) and whole-nose dose (Tables 3 and Tables 4) indicates that fluxes of equal magnitude do not exactly overlay the same anatomical regions of the nasal cavity in each individual. This implies that specific anatomical regions subtended by maximum flux could be offset from one individual to another. Such an offset that involved target tissues of a reactive gas, such as the olfactory epithelium, could result in more variability in the dose to these target tissues despite the similarity of the overall dose to the nasal cavity. More refined individual anatomic maps of epithelial tissues would be required to further investigate such a possibility.

The rates of gas absorption in the 7- and 8-yr-old children were similar to those predicted for the adults (Tables 3 and Tables 4; Figure 6). It is fascinating that nasal doses are similar in children and adults given that inhalation rates are smaller in children. Children inhale less gas, but their nasal surface area is smaller (Table 1), leading to doses (per unit area) that are similar to those observed in adults. Our prediction of comparable nasal doses of inhaled gases in children and adults is supported by Sarangapani et al. (2003) and Ginsberg et al. (2005). These researchers applied models based on the RfC methodology (U.S. EPA, 1994) to calculate average doses to the extrathoracic airways. No significant differences were predicted from 1 mo to 75 yr of age. In addition, our simulations revealed that the distribution of nasal surface area by wall flux magnitude is similar in the two age groups (Figure 7; Table 5). These findings contrast with the common view that respiratory doses of toxicants are greater in children than in adults (Wild & Kleinjans, 2003; Ginsberg et al., 2005). Although there is evidence suggesting that lung doses of inhaled particles are greater in children (Ginsberg et al., 2005; Becquemin et al., 1991), our results suggest that nasal doses of inhaled reactive gases are similar in the two age groups.

In interpreting these results, the reader should be aware of the following limitations of our study. First, our gas transport simulations are not representative of a specific water-soluble and reactive gas but are characteristic of gases with moderate to high nasal uptake. The simulations do not account for the nonuniform distribution of epithelial types, enzymes, glands and other cellular metabolic or clearance machinery that would also affect localized flux. A higher interhuman variability in nasal dose would be expected if such toxicodynamic effects were taken into account. By assuming a constant boundary condition over the entire nasal wall, the simulations focused on the effects of anatomy on flux distribution during resting breathing. Second, the small size of our sample did not allow for a statistical analysis. Third, children younger than 7 yr old were not studied. Fourth, our model assumed a rigid nasal geometry, while the nasal mucosa is a dynamic entity that can swell/congest in response to toxic stimuli.

The strength of the present study is fivefold. First, the CFD technique provided a comprehensive description of the wall fluxes along the nasal walls. The simulations revealed a highly nonuniform distribution of fluxes, with maximum fluxes up to nine times greater than average values. Second, although the inclusion of seven subjects was not sufficient for statistical analysis, this study represents a significant increase in the number of nasal geometries investigated in the CFD literature, where most papers examine a single nasal geometry (Elad et al., 2006; Keyhani et al., 1995; Lindemann et al., 2005a, 2005b; Subramaniam et al., 1998; Zamankhan et al., 2006; Zhao et al., 2004). Third, to the best of our knowledge, this is the first CFD article to present airflow simulations in the noses of children. Fourth, our simulations predicted no differences in the nasal dosimetry of reactive, water-soluble gases between children and adults, suggesting that the risk factor of 10 typically used to accommodate interhuman variability is adequate. Fifth, the current study points out to important areas of future research that must be done to determine an appropriate risk factor to account for interhuman variability in risk assessment of inhaled toxic gases.

Conclusions

In summary, the results reported in this study suggest that the differential in risk due to differences in dosimetry between children and adults exposed to toxic gases may not be extensive, i.e., less than the factor of 10 typically used to accommodate interhuman variability. More studies are needed to confirm this prediction. In particular, future studies should investigate larger cohorts that include children of different ages, especially infants. Patients with anatomical abnormalities, such as septal perforations (Pless et al., 2004), should also be included for a more complete assessment of the anatomical variability in the adult population. Finally, interhuman variability in toxicodynamics can be investigated by taking into account the distribution of epithelial types, enzymes, and metabolites within the nasal passages.

Appendix

The conservation of mass and momentum for laminar, incompressible flow is described, respectively, by the Navier–Stokes equations

$$\nabla\cdot\vec{u}=0, \tag{5}$$

$$\rho\frac{\partial\vec{u}}{\partial t}+\rho(\vec{u}\cdot\nabla)\vec{u}=-\nabla p+\mu\nabla^2\vec{u} \tag{6}$$

where $\vec{u}=\vec{u}(x,y,z,t)$ is the velocity vector, t is time, p is pressure, ρ is fluid density, and μ is dynamic viscosity (Çengel & Cimbala, 2006; White, 2008). In our simulations we adopted ρ = 1.204 kg/m^3 and μ = 1.825 × 10^{-5} kg/ms (Çengel & Cimbala, 2006).

The transport of inhaled gas is governed by the convection–diffusion equation

$$\frac{\partial}{\partial t}c+(\vec{u}\cdot\nabla)c=D\nabla^2c \tag{7}$$

where $c = c\ (x,y,z,t)$ is the gas concentration in air and D = 1.5 × 10^{-5} m^2/s is the mass diffusivity of the gas in air (Hobler, 1966; Kimbell et al., 2001a).

Steady-state versions of these equations were solved on a dual-processor workstation (Dell Precision, Intel Xeon 3.60 GHz, 3.93 GB of RAM) using Fluent 6.2.16 (Fluent, Inc., Lebanon, NH). Fluent uses the finite volume method to solve the differential equations numerically. The segregated solver with SIMPLEC pressure–velocity coupling and second-order, upwind discretization were utilized for solution of the

equations. Since the physical properties of the air–gas mixture were assumed constant, an uncoupled solution strategy was employed, namely, the flow field was obtained first and then the convection–diffusion equation was solved.

The following boundary conditions were used to determine the air flow field: (a) no-slip (zero velocity) at the airway walls, (b) mass-flow inlet at the nostrils, and (c) pressure outlet at the nasopharynx. The boundary conditions to simulate gas uptake were described in the Methods section. Fluent 6.2 does not provide the option of setting a boundary condition of the type $\text{Flux} = -D(\vec{n}\times\nabla c)_{\text{wall}} = k(c)_{\text{wall}}$ for species transport. Therefore, a User-Defined Scalar was defined in Fluent and the boundary condition applied through a User-Defined Function. Fluent took ~8.5 h of computing time (~1300 iterations) to solve the equations for a mesh with 3.1 million elements. Convergence was confirmed by small residuals (continuity: $<10^{-4}$; velocities: $<10^{-5}$; convection diffusion equation: $<3\times10^{-5}$; user-defined scalar: $<3\times10^{-7}$) and by monitoring the gas concentration at the outlet surface for stabilization.

Note

1 According to the NRC report on Science and Judgment in Risk Assessment (NRC, 1994, p. 28), "[Default procedures] are generic approaches, based on general scientific knowledge and policy judgment, that are applied to various elements of the risk assessment process when specific scientific information is not available."

Acknowledgement

We thank Darin Kalisak, Regina Richardson, and Dr. Grace Kepler for their contributions to this project. We are also grateful to Dr. Todd Yokley, Dr. Brent Senior, Dr. Rose Eapen, Dr. Dário Martins, and Dr. Neil Bailie for the provision and medical evaluation of CT scans and Dr. Kambiz Nazridoust for assistance with Fluent. This study was funded by the U.S. EPA, project numbers EP05C000009 and EP06C000405, and by the American Chemistry Council.

The views expressed in this article are those of the authors and do not necessarily reflect the views or policies of the U.S. Environmental Protection Agency.

***Declaration of interest*:** The authors report no conflicts of interest.

References

Aitken, M. L., Franklin, J. L., Pierson, D. J., Schoene, R. B. 1986. Influence of body size and gender on control of ventilation. *J. Appl. Physiol.* 60:1894–1899.

Andersen, M. E., Jarabek, A. M. 2001. Nasal tissue dosimetry—Issues and approaches for "Category I" gases: A report on a meeting held in Research Triangle Park, NC, February 11–12, 1998. *Inhal. Toxicol.* 13:415–435.

Arcus-Arth, A.,Blaisdell, R. J. 2007. Statistical distributions of daily breathing rates for narrow age groups of infants and children. *Risk. Anal.* 27:97–110.

Beals, J. A., Funk, L. M., Fountain, R.,Sedman, R. 1996. Quantifying the distribution of inhalation exposure in human populations: distribution of minute volumes in adults and children. *Environ. Health Perspect.* 104:974–979.

Becquemin, M. H., Swift, D. L., Bouchikhi, A., Roy, M., Teillac, A. 1991. Particle deposition and resistance in the noses of adults and children. *Eur. Respir. J.* 4:694–702.

Bennett, W. D., Zeman, K. L. 2004. Effect of body size on breathing pattern and fine-particle deposition in children. *J. Appl. Physiol.* 97:821–826.

Bide, R. W., Armour, S. J., Yee, E. 2000. Allometric respiration/body mass data for animals to be used for estimates of inhalation toxicity to young adult humans. *J. Appl. Toxicol.* 20:273–290.

Brochu, P., Ducré-Robitaille, J.-F., Brodeur, J. 2006. Physiological daily inhalation rates for free-living individuals aged 1 month to 96 years, using data from doubly labeled water measurements: A proposal for air quality criteria, standard calculations and health risk assessment. *Hum. Ecol. Risk Assess.* 12:675–701.

Carey, S. A., Minard, K. R., Trease, L. L., Wagner, J. G., Garcia, G. J., Ballinger, C. A., Kimbell, J. S., Plopper, C. G., Corley, R. A., Postlethwait, E. M., Harkema, J. R. 2007. Three-dimensional mapping of ozone-induced injury in the nasal airways of monkeys using magnetic resonance imaging and morphometric techniques. *Toxicol. Pathol.* 35:27–40.

Çengel, Y. A., Cimbala, J. M. 2006. *Fluid mechanics: Fundamentals and applications*. New York: McGraw-Hill.

Cohen Hubal, E. A., Kimbell, J. S.,Fedkiw, P. S. 1996. Incorporation of nasal-lining mass-transfer resistance into a CFD model for prediction of ozone dosimetry in the upper respiratory tract. *Inhal. Toxicol.* 8:831–857.

Dahl, A. R. 1990. Dose concepts for inhaled vapors and gases. *Toxicol. Appl. Pharmacol.* 103:185–197.

Dorne, J. L. 2004. Impact of inter-individual differences in drug metabolism and pharmacokinetics on safety evaluation. *Fundam. Clin. Pharmacol.* 18:609–620.

Elad, D., Liebenthal, R., Wenig, B. L., Einav, S. 1993. Analysis of air flow patterns in the human nose. *Med. Biol. Eng. Comp.* 31:585–592.

Elad, D., Naftali, S., Rosenfeld, M., Wolf, M. 2006. Physical stresses at the air–wall interface of the human nasal cavity during breathing. *J. Appl. Physiol.* 100:1003–1010.

Fluent, Inc. *Fluent 6.2 user's guide.* Lebanon, NH: Fluent, Inc..

Garcia, G. J. M., Bailie, N., Martins, D. A., Kimbell, J. S. 2007. Atrophic rhinitis: A CFD study of air conditioning in the nasal cavity. *J. Appl. Physiol.* 103:1082–1092.

Ginsberg, G. L., Foos, B. P., Firestone, M. P. 2005. Review and analysis of inhalation dosimetry methods for application to children's risk assessment. *J. Toxicol. Environ. Health A* 68:573–615.

Guilmette, R. A., Cheng, Y. S., Griffith, W. C. 1997. Characterising the variability in adult human nasal airway dimensions. *Ann. Occup. Hyg.* 41:491–496.

Han, J. N., Stegen, K., Cauberghs, M., Van de Woestijne, K. P. 1997. Influence of awareness of the recording of breathing on respiratory pattern in healthy humans. *Eur. Respir. J.* 10:161–166.

Hobler, T. 1966. *Mass transfer and absorbers.* New York: Pergamon Press.

International Commission on Radiological Protection1994. Publication 66. Human respiratory tract model for radiological protection. *Ann. ICRP 24.* Oxford: Pergamon Press.

Keyhani, K., Scherer, P. W., Mozell, M. M. 1995. Numerical simulation of airflow in the human nasal cavity. *J. Biomech. Eng.* 117:429–441.

Kimbell, J. S., Gross, E. A., Joyner, D. R., Godo, M. N., Morgan, K. T. 1993. Application of computational fluid dynamics to regional dosimetry of inhaled chemicals in the upper respiratory tract of the rat. *Toxicol. Appl. Pharmacol.* 121:253–263.

Kimbell, J. S., Subramaniam, R. P., Gross, E. A., Schlosser, P. M., Morgan, K. T. 2001a. Dosimetry modeling of inhaled formaldehyde: Comparisons of local flux predictions in the rat, monkey, and human nasal passages. *Toxicol. Sci.* 64:100–110.

Kimbell, J. S., Overton, J. H., Subramaniam, R. P., Schlosser, P. M., Morgan, K. T., Conolly, R. B., Miller, F. J. 2001b. Dosimetry modeling of inhaled formaldehyde: binning nasal flux predictions for quantitative risk assessment. *Toxicol. Sci.* 64:111–121.

Lang, J. 1989. *Clinical anatomy of the nose, nasal cavity and paranasal sinuses.* New York: Thieme Medical.

Layton, D. W. 1993. Metabolically consistent breathing rates for use in dose assessments. *Health Phys.* 64:23–36.

Lehmann, G. 1935. The dust filtering efficiency of the human nose and its significance in the causation of silicosis. *J. Ind. Hyg.* 17:37–40.

Lindemann, J., Brambs, H. J., Keck, T., Wiesmiller, K. M., Rettinger, G., Pless, D. 2005a. Numerical simulation of intranasal airflow after radical sinus surgery. *Am. J. Otolaryngol.* 26:175–180.

Lindemann, J., Keck, T., Wiesmiller, K. M., Rettinger, G., Brambs, H. J.,Pless, D. 2005b. Numerical simulation of intranasal air flow and temperature after resection of the turbinates. *Rhinology* 43:24–28.

Morgan, K. T., Kimbell, J. S., Monticello, T. M., Patra, A. L., Fleishman, A. 1991. Studies of inspiratory airflow patterns in the nasal passages of the F344 rat and rhesus monkey using nasal molds: Relevance to formaldehyde toxicity. *Toxicol. Appl. Pharmacol.* 110:223–240.

Morgan, K. T. 1994. Nasal dosimetry, lesion distribution, and the toxicologic pathologist: A brief review. *Inhal. Toxicol.* 6(suppl.):41–57.

Morris, J. B. 1994. In vivo measurements of uptake. *Inhal. Toxicol.* 6 (suppl.):99–111.

Naya, M., Nakanishi, J. 2005. Risk assessment of formaldehyde for the general population in Japan. Regul. *Toxicol. Pharmacol.* 43:232–248.

National Research Council. 1994. Science and judgment in risk assessment. *Committee on Risk Assessment of Hazardous Air Pollutants, Board on Environmental Studies and Toxicology, Commission on Life Sciences.* Washington, DC: National Academies Press.

Overton, J. H., Kimbell, J. S., Miller, F. J. 2001. Dosimetry modeling of inhaled formaldehyde: the human respiratory tract. *Toxicol. Sci.* 64:122–134.

Pelekis, M., Nicolich, M. J., Gauthier, J. S. 2003. Probabilistic framework for the estimation of the adult and child toxicokinetic intraspecies uncertainty factors. *Risk. Anal.* 23:1239–1255.

Perez, W., Tobin, M. J. 1985. Separation of factors responsible for change in breathing pattern induced by instrumentation. *J. Appl. Physiol.* 59:1515–1520.

Pless, D., Keck, T., Wiesmiller, K. M., Lamche, R., Aschoff, A. J., Lindemann, J. 2004. Numerical simulation of airflow patterns and air temperature distribution during inspiration in a nose model with septal perforation. *Am. J. Rhinol.* 18:357–362.

Sarangapani, R., Gentry, P. R., Covington, T. R., Teeguarden, J. G., Clewell, H. J. 2003. Evaluation of the potential impact of age- and gender-specific lung morphology and ventilation rate on the dosimetry of vapors. *Inhal. Toxicol.* 15:987–1016.

Schroeter, J. D., Kimbell, J. S., Bonner, A. M., Roberts, K. C., Andersen, M. E., Dorman, D. C. 2006a. Incorporation of tissue reaction kinetics in a computational fluid dynamics model for nasal extraction of inhaled hydrogen sulfide in rats. *Toxicol. Sci.* 90:198–207.

Schroeter, J. D., Kimbell, J. S., Andersen, M. E., Dorman, D. C. 2006b. Use of a pharmacokinetic-driven computational fluid dynamics model to predict nasal extraction of hydrogen sulfide in rats and humans. *Toxicol. Sci.* 94:359–367.

Segal, R. A., Kepler, G. M., Kimbell, J. S. 2008. Effects of Differences in Nasal Anatomy on Airflow Distribution: A Comparison of Four Individuals at Rest. *Annals of Biomedical Engineering* 36:1870–1882.

Subramaniam, R. P., Richardson, R. B., Morgan, K. T., Kimbell, J. S., Guilmette, R. A. 1998. Computational fluid dynamics simulations of inspiratory airflow in the human nose and nasopharynx. *Inhal. Toxicol.* 10:91–120.

Taylor, A. B. 2006. *Three-dimensional computational fluid dynamics simulations of ozone uptake in the respiratory tract.* PhD thesis, College of Engineering, Pennsylvania State University.

U.S. Environmental Protection Agency 1994. Methods for derivation of inhaled reference concentrations and application of inhalation dosimetry. Environmental Criteria and Assessment Office, Office of Health and Environmental Assessment, Cincinnati, OH. EPA/600/8-90/066F. Available from the National Technical Information Service, Springfield, VA, PB2000-500023, and online at http://www.epa.gov/ncea.

Wexler, D., Segal, R., Kimbell, J. 2005. Aerodynamic effects of inferior turbinate reduction—Computational fluid dynamics simulation. *Arch. Otolaryngol. Head Neck Surg.* 131:1102–1107.

White, F. M. 2008. *Fluid mechanics.* New York: McGraw-Hill.

Wild, C. P., Kleinjans, J. 2003. Children and increased susceptibility to environmental carcinogens: Evidence or empathy? *Cancer Epidemiol. Biomarkers* 12:1389–1394.

Yokley, T. R. 2006. *The functional and adaptive significance of anatomical variation in recent and fossil human nasal passages.* PhD thesis, Duke University, Durham, NC.

Zamankhan, P., Ahmadi, G., Wang, Z. C., Hopke, P. K., Cheng, Y. S., Su, W. C., Leonard, D. 2006. Airflow and deposition of nano-particles in a human nasal cavity. *Aerosol Sci. Technol.* 40:463–476.

Zhao, K., Scherer, P. W., Hajiloo, S. A.,Dalton, P. 2004. Effect of anatomy on human nasal air flow and odorant transport patterns: Implications for olfaction. *Chem. Senses* 29:365–379.